

1 Supplementary Information for:
2 Social Mixing and Network Characteristics of
3 COVID-19 Patients Before and After
4 Widespread Interventions: A
5 Population-based Study

6 Yuncong He^{1†}, Leonardo Martinez^{2†}, Yang Ge^{3†}, Yan
7 Feng^{4†}, Yewen Chen^{5†}, Jianbin Tan¹, Adrianna
8 Westbrook⁵, Changwei Li⁶, Wei Cheng⁴, Feng Ling⁴, Huimin
9 Cheng⁷, Shushan Wu⁷, Wenxuan Zhong⁷, Andreas
10 Handel⁵, Hui Huang^{8*}, Jimin Sun^{4*} and Ye Shen^{5*}

11 ¹School of Mathematics, Sun Yat-sen University, Guangzhou,
12 510275, Guangdong, China.

13 ²Department of Epidemiology, School of Public Health, Boston
14 University, Boston, 02118, Massachusetts, United States.

15 ³School of Health Professions, University of Southern Mississippi,
16 Hattiesburg, 39402, Mississippi, United States.

17 ⁴Zhejiang Provincial Center for Disease Control and Prevention,
18 Hangzhou, 310051, Zhejiang, China.

19 ⁵Department of Epidemiology and Biostatistics, College of Public
20 Health, University of Georgia, Athens, 30602, Georgia, United
21 States.

22 ⁶Department of Epidemiology, Tulane University School of Public
23 Health and Tropical Medicine, New Orleans, 70112, Louisiana,
24 United States.

25 ⁷Department of Statistics, University of Georgia, New Athens,
26 30602, Georgia, United States.

27 ⁸Center for Applied Statistics and School of Statistics, Renmin
28 University of China, Beijing, 100872, China.

*Corresponding author(s). E-mail(s):

huangh89@mail.sysu.edu.cn; jmsun@cdc.zj.cn; yeshen@uga.edu;

†These authors contributed equally to this work.

Data source

We collected individual-level data on 1349 SARS-CoV-2 infections during the major outbreak in Zhejiang province, China, from January 8th to February 23rd, 2020 [1, 2]. The data contain comprehensive information of each case, such as their demographical information and epidemiological linkage to others identified through contact tracing efforts. The resulted infector-infectee transmission pairs thereby inherently contain the nature of a directed transmission network. Precisely, started from each indexed case, edges consecutively direct out to the secondary infections, which ultimately form a cluster or a “component” in the terminology of network science. The infector-infectee transmission pairs form a transmission network combining such clusters. The nodes and edges inside are unlikely to be homogeneous, and the topological characteristics of the networks across periods are also distinct. To better understand the patterns and drivers of such heterogeneity, we analyze four fundamental graphical measures introduced below, both statically and dynamically.

The personal information for each case includes age, gender, guardians (if applicable), household information, household and occupational location, the severity of infection, potential exposures, travel history to other areas, date of symptom onset, and date of laboratory-confirmation. Potential exposures are recorded in detailed texts where we extracted names and types of exposures. All epidemiological information and laboratory confirmation were collected by specialists in provincial or municipal CDC or hospitals in Zhejiang. Extra efforts were conducted to correct typographical errors (such as names in the same pronunciation) and explore additional information such as family relation that is missed in raw records.

Methods

Notation of network and definitions of network characteristics

We use a 2-tuple (N, g) to represent a network object, where N is the set of indexes of nodes and the adjacency matrix g is a real-valued $n \times n$ matrix, in which entry g_{ij} represents the relation between i and j . In a transmission network with specified transmission directions, $g_{ij} = 1$ means that i is the source case of j and j is the secondary case of i . The out-degree of a node is the number of edges directed out from it and the in-degree of a node is the number of edges that ends with it. We let d_i^+ and d_i^- denote the out-degree

67 and in-degree of the i th node, respectively. Thus if $d_i^+ > 0$ and $d_i^- = 0$, the
 68 i th node is an indexed case which is the origin of a cluster. On the other
 69 hand, if $d_i^+ = 0$ and $d_i^- > 0$, the i th node is a terminal case that induces
 70 no other secondary case. If both $d_i^+ = 0$ and $d_i^- = 0$, the i th node does not
 71 belong to any cluster, and it is marked as a singleton in the network. We let S
 72 denote the set of singletons. The reasons for a node becoming a singleton are
 73 twofold. For one thing, it was an imported case and did not infect anybody.
 74 For another, the transmission linkage of it was inexplicit, and epidemiologists
 75 were not able to identify neither the source case nor secondary cases of it. For
 76 example, there was a large outbreak within a prison, but we were unable to
 77 identify an explicit transmission chain, and thus, most of the involved cases
 78 were considered singletons. In calculating network characteristics, we neglect
 79 the existence of singletons inside; i.e., we focus on the sub-network $N \setminus S$.

80 Throughout this article, we mainly consider four basic graphical mea-
 81 sures of the transmission network: 1) Average out-degree, 2) average shortest
 82 path length, 3) diameter of clusters, and 4) sizes of clusters, which would
 83 characterize the number of secondary cases, the cohesion of the transmission
 84 occurrence, the generations of the epidemic spread and the developed size for
 85 one clustered epidemic event, respectively. The average out-degree is the sum
 86 of out-degree for non-singleton cases divided by the total number of them,
 87 that is $\sum_{j \in N \setminus S} d_j^+ / |N \setminus S|$, where $|\cdot|$ denotes the cardinality of a set. For
 88 the average shortest path length (ASPL), we firstly define that $\text{path}(i, j) = 1$
 89 if there exists a directed path beginning from the i th and ending in the j th
 90 nodes, otherwise $\text{path}(i, j) = 0$. Among all paths, the distance between the
 91 i th and the j th nodes, $\text{dist}(i, j)$ is defined as the length of their shortest path
 92 (i.e., geodesic). If $\text{path}(i, j) = 0$, we assume the distance between them is 0.
 93 The average shortest path length is defined as [3]

$$\text{ASPL} = \frac{\sum_{i,j \in N, i \neq j} \text{dist}(i, j)}{\sum_{i,j \in N, i \neq j} \text{path}(i, j)} \quad (\text{S1})$$

94 Moreover, betweenness centrality of node v is defined as

$$C_B(v) = \sum_{i,j: i \neq j \neq v} \frac{g_{ivj}}{g_{ij}} \quad (\text{S2})$$

95 where g_{ij} is the total number of shortest paths from node i to node j
 96 and g_{ivj} is the total number of shortest paths from node i to node j via
 97 node v . Therefore, $C_B(v)$ quantifies the information transportation that passes
 98 through node v . Furthermore, information is originated from instead of trans-
 99 porting through the source node of a tree-shaped network, the betweenness
 100 centrality of it is always zero. Similarly, the betweenness centrality of a terminal
 101 node inside a tree-shaped network is also zero. Therefore, in a transmis-
 102 sion network (composed of tree-shaped sub-networks), only the intermediate
 103 nodes between the source and terminal nodes contribute to the measure of
 104 betweenness.

105 The diameter of a connected transmission network is the maximum distance
106 within it; i.e., the distance from the indexed case to the farthest terminal case.
107 In the context of epidemiology, the diameter of a transmission network is the
108 maximum generation of the virus spread within it. Since the whole transmis-
109 sion network can be decomposed into a collection of clusters or components,
110 we calculate the average diameter of clusters by averaging the diameter of each
111 cluster. Lastly, the size of a sub-network is the number of nodes within it. Thus,
112 the average size of clusters is calculated by averaging the sizes of clusters.

113 Agent-based transmission network model for simulations

114 A detailed description of how we build an agent-based transmission network
115 model is presented in the main text. Here we provide supplementary materials
116 on its settings. Key parameters for the outbreak reconstruction are summa-
117 rized in Table S1. As described in the main text, we first build a social network
118 considering the household, geographical, and random connections between peo-
119 ple. Specifically, we utilize our observational data to give realistic settings for
120 parameters such as household size and family-based age distribution. In addi-
121 tion, we construct a social connection network consistent with the age-specific
122 contact rates matrix explored in detail by Zhang et al. [4] and assign weights
123 in different connections.

124 In terms of the transmission processes, we consider both pre-symptomatic
125 infectiousness and post-symptomatic viral shedding. More precisely, patients
126 are able to transmit COVID-19 before showing symptoms [5] (pre-symptomatic
127 infectiousness) and will lose infectiousness afterwards due to insufficient viral
128 loading [5, 6]. Thus, we assume five compartments in our model: suscep-
129 tible, exposed, pre-symptomatic infectious, post-symptomatic infectious and
130 removed state. Every node is initially susceptible. After exposure to known
131 infectious cases, a node has a probability $(1 - (1 - \beta)^n$ in the main-text) to be
132 infected and will then be transferred to the exposed state. In the exposed state,
133 cases are non-infectious. After a period of time (we assume it as a proportion
134 of the incubation period, the duration from being infected to symptom onset),
135 cases will be transferred to the pre-symptomatic infectious state. Afterwards,
136 cases will show symptoms and move to the post-symptomatic infectious state.
137 As long as they develop symptoms, they will be assigned a removal period,
138 the duration between symptom onset and isolation. After a removal period,
139 cases will be quarantined and no longer participate in the transmission pro-
140 cesses, i.e., move to the removed state. Note that in very early stage of the
141 outbreak, the speed of case finding is relatively slow. Therefore, the removal
142 period can be longer than the post-symptomatic infectious period as cases
143 could be physically free while already losing their infectiousness capabilities.
144 Settings for those periods as well as age-dependent heterogeneity are in accor-
145 dance with some previous studies [5–7]. For the removal of infected cases,
146 we set the removal period based on our observational data (see Fig. S8 (a)).
147 Moreover, we incorporated a dynamic change of contact pattern through the
148 pre-outbreak, lockdown, and resumption phases based on previously reported

149 contact matrices observed during the pre-outbreak and outbreak periods [4]
 150 (see *Construction of daily age-specific contact matrix*, Fig. S2 and Fig. S3).

151 Construction of daily age-specific contact matrix

152 According to Zhang et al. [4], we can get the age-specific contact matrix for
 153 both baseline period and outbreak period, denoted by c_{base} and c_{outbreak} . How-
 154 ever, neither the intermediate state in between nor the contact pattern in the
 155 post-lockdown period was observed. Therefore, we assume that it decrease as a
 156 time-dependent function following Tan et al. [8] (Fig. S3). At the beginning, we
 157 assume the contact rate declined in a very small scale (ϵ) before January 10th
 158 (3 days from January 8th) and started to drop afterwards. Zhejiang provincial
 159 government upgraded its infectious disease alert category to the highest level
 160 on January 23rd, 2020, we assumed that the social contact frequency dropped
 161 to the lowest level afterwards. The provincial government started the reopen-
 162 ing on February 10th, 33 days from January 8th, after which the social contact
 163 frequency increased. Because COVID-19 cases were still being reported spo-
 164 radically, we assumed the social contact frequency, in the following one month,
 165 equal to an average of the contact levels in the baseline period and the outbreak
 166 period. Briefly, let $c^{(d)}$ be the contact matrix in the d day. Then $c^{(0)} = c_{\text{base}}$,
 167 $c^{(d)} = c_{\text{outbreak}}$ for $16 \leq d \leq 32$ and $c^{(d)} = (c_{\text{base}} + c_{\text{outbreak}})/2$ for $d \geq 63$. We
 168 denote the average contact number of the i th age group to the j th age group
 169 at time d as $c_{ij}^{(d)}$. For $1 \leq d \leq 16$, the monotonic decline function followed a
 170 logistic curve given by the following equation:

$$c_{ij}^{(d)} = c_{ij}^{(0)} \left(\frac{1 - \eta_{ij}}{1 + \exp(\lambda_m(d - t_0 - m/2))} + \eta_{ij} \right) \quad (\text{S3})$$

171 Here, if λ_m is chosen as $2 \log(\epsilon/(1 - \epsilon))/m$ and ϵ is sufficiently small (e.g.
 172 $\epsilon = 0.01$), m could be viewed as the duration of the decreasing process [8]
 173 (as illustrated in Fig. S2). $\eta_{ij} = c_{ij}^{(16)}/c_{ij}^{(0)}$ is the percentage of decrease. As
 174 discussed above, we set $m = 13$, $t_0 = 3$. On the other hand, in terms of the
 175 resumption process, for $32 \leq d \leq 62$, we invert the decreasing process by:

$$c_{ij}^{(d)} = c_{ij}^{(63)} \left(\frac{1 - \gamma_{ij}}{1 + \exp(\lambda_m(62 - d - m/2))} + \gamma_{ij} \right) \quad (\text{S4})$$

176 where $m = 30$ with λ_m as defined above and $\gamma_{ij} = c_{ij}^{(32)}/c_{ij}^{(62)}$. In a nutshell, we
 177 can get a series of contact matrices for every day d ($c^{(d)}$) presented in Fig. S3.

178 Exploration and supporting results

179 Graphical characteristics of the observed transmission 180 data

181 We collected data on 1349 confirmed SARS-CoV-2 infections identified in
 182 Zhejiang Province as well as their baseline information and epidemiological

183 tracing notes. From information collected through contact tracing, we par-
184 tially recovered the infector-infectee transmission chains between cases. If one
185 case had more than one potential source of infection, we sampled only one.
186 Sensitivity results are presented in *variation of sampling a source case*. There-
187 after, a transmission network can be constructed by combining all transmission
188 pairs. We then computed four basic graphical measures to assess the transmis-
189 sion network quantitatively: 1) Average out-degree, 2) average shortest path
190 length, 3) diameter of clusters, and 4) sizes of clusters. Among them, there
191 exists heterogeneity related to demographical factors such as age and house-
192 hold transmission. Relatively older adult cases accounted for more significant
193 contributions than younger adult and adolescent cases in the transmission pro-
194 cesses (top-right corner in Fig. S4 (a)). Notably, the average out-degree (i.e.,
195 number of secondary infections) induced by cases aged between 40 and 59 is
196 considerably higher than that induced by cases from other age groups (Fig. S4
197 (b)). Furthermore, those aged between 40 and 59 were more frequently identi-
198 fied as the indexed cases in the transmission network, while cases from other
199 age groups were substantially more likely to be positioned as the terminal
200 cases. In terms of household transmission, 54.5% of the terminal transmission
201 occurred within the household, while household transmission only accounted
202 for 39.3% of non-terminal transmission.

203 **Dynamic epidemiological and graphical characteristics of** 204 **the transmission network**

205 Across periods before and during the outbreak (that is period I and period
206 II), there existed a quantity of change both on epidemiological and graphical
207 aspects. First, the average removal period (the duration from symptom onset
208 to isolation, which reflects the speed of case finding) was decreasing over time,
209 starting from nearly 20 days and ending with virtually zero (Fig. S8 (a)). In
210 aggregation, the average removal period in period I was 6.41 days, while in
211 period II, it was 4.18 days. Moreover, the curve of imported cases over time
212 peaked at the declaration of lock-down, with most of them from period I
213 (Fig. S8 (b)). On a graphical aspect, the secondary infection induced by cases
214 of all ages showed a clear distinction between periods (Fig. S6 (b)). Cases
215 aged between 40 and 59, the age groups with the largest average out-degree
216 in period I, encountered a considerable decrease in this quantity in period
217 II. However, for all other ages, the secondary infection increased. Their wax
218 and wane jointly resulted in a relatively homogeneous distribution in average
219 out-degree across age groups in period II. Besides, the heterogeneity of cases'
220 location in the network related to their age also changed by periods (Fig. S6
221 (a)). Except in those below 20, cases belonging to other age groups had an
222 increasing proportion as an indexed case between periods I and II. Conversely,
223 the proportion as a terminal case dropped in nearly all age groups. Household
224 transmission often resulted in terminal transmission during both periods, but
225 that proportion considerably rose from period I to period II. In addition, from
226 period I to II, some graphical measures such as average out-degree, average

227 shorted path length, and the average size of clusters encountered noticeable
228 recession. Both the large-spreading events (each with an out-degree at least
229 3) and large clusters (with a size of at least 5) became less common in period
230 II. Most of the shortest path length between cases concentrated below 2, also
231 suggesting that clusters became much more cohesive around their indexed
232 cases and less forked.

233 Reconstruction of the transmission network

234 Using the agent-based transmission network model described in the main text
235 as well as *Agent-based transmission network model for simulations* under real-
236 istic settings given in Table S1, we reconstructed a transmission network for
237 the outbreak in Zhejiang from January 8th to February 23rd. From Fig. S9,
238 the daily number of the new-onset cases in reconstruction fitted well to the
239 observed one.

240 Sensitivity analysis on the split-point of time 241 periods

242 January 20th as the split-point

243 We chose the time before January 20th as the first period and the time after
244 January 21st as the second period and repeat the analysis on the main text.
245 The results show that some network attributes significantly changed across
246 periods. In details, the proportion of singletons significantly increased from
247 32.4% (95% CI: 27.6%, 37.4%) to 58.8% (95% CI: 55.4%, 62.7%) ($p < 0.001$);
248 average out-degree from 0.77 (95% CI: 0.69, 0.83) to 0.66 (95% CI: 0.62, 0.70)
249 ($p = 0.012$); average shortest path length from 1.63 (95% CI: 1.25, 1.77) to 1.17
250 (95% CI: 1.10, 1.21) ($p = 0.012$); average diameter of clusters from 1.41 (95%
251 CI: 1.23, 1.55) to 1.23 (95% CI: 1.15, 1.30) ($p = 0.042$); average size of clusters
252 from 4.41 (95% CI: 3.19, 5.84) to 2.97 (95% CI: 2.62, 3.32) ($p = 0.0122$); the
253 proportion of household transmission from 45.7% (95% CI: 38.6%, 54.0%) to
254 59.4% (95% CI: 52.0%, 67.7%) ($p = 0.042$), average removal period from 10.29
255 days (SE: 0.28) to 4.48 days (SE: 0.11) ($p < 0.001$); the number of clusters
256 increased from 75 to 119. Only one attribute's change was statistically insignif-
257 icant, the proportion of super-spreaders from 7.7% (95% CI: 5.1%, 9.3%) to
258 4.8% (95% CI: 3.0%, 6.4%) ($p = 0.065$).

259 Compared to the result on the main text using January 23 as the split-
260 point, on a significance level of 0.05, there are two statistically different results:
261 the decrease of proportion of super-spreaders became insignificant and the
262 decrease of average diameter of clusters become significant. This is because
263 after re-allocating the time between January 21st and January 23rd into period
264 II, the number of super-spreading events in period II and the average diameter
265 of clusters in period I increased significantly.

February 1st as the split-point

We chose the time before February 1st as the first period and the time after February 2nd as the second period and repeat the analysis on the main text. The results show that nearly all network attributes insignificantly changed across periods. In details, the proportion of singletons significantly increased from 45.6% (95% CI: 42.4%, 48.6%) to 85.5% (95% CI: 79.1%, 91.1%) ($p < 0.001$); the number of clusters largely dropped from 186 to 8. The change of other attributes was statistically insignificant: the proportion of super-spreaders from 6.3% (95% CI: 4.8%, 7.4%) to 0.0% (95% CI: 0.0%, 0.0%) ($p = 0.3453$); average out-degree from 0.72 (95% CI: 0.67, 0.77) to 0.56 (95% CI: 0.50, 0.61) ($p = 0.158$); average shorted path length from 1.47 (95% CI: 1.25, 1.65) to 1.00 (95% CI: 1.00, 1.00) ($p = 0.137$); average betweenness centrality from 0.52 (95% CI: 0.22, 0.89) to 0.00 (95% CI: 0.00, 0.00) ($p = 0.179$); average diameter of clusters from 1.32 (95% CI: 1.23, 1.42) to 1.00 (95% CI: 1.00, 1.00) ($p = 0.137$); average size of clusters from 3.59 (95% CI: 3.05, 4.34) to 2.25 (95% CI: 2.00, 2.57) ($p = 0.147$); the proportion of household transmission from 52.0% (95% CI: 44.2%, 60.0%) to 60.0% (95% CI: 36.4%, 94.7%) ($p = 0.749$). Average removal period dropped significantly from 6.63 days (SE: 0.13) to 2.06 days (SE: 0.13) ($p < 0.001$).

Compared to the result on the main text using January 23 as the split-point, on a significance level of 0.05, nearly all statistically significant results changed to as insignificant. In period II (after February 1st), the total number of cases and clusters both dropped significantly, which could have caused reduced statistical powers.

Variation of sampling a source case

We also conduct a sensitivity analysis on assessing the variation of sampling a source case. There are 43 cases with more than one potential source cases. For such cases, we randomly sample one "true" parent among all potential source cases and repeat the analysis on the main text.

Among 100 repetitions, results on comparison across periods in the main text are consistent except the proportion of superspreaders, average shortest path length and average diameter of clusters. 29% of the comparisons on the proportion of superspreaders, 19% on the average shortest path length and 65% on the average diameter of clusters vary from the results in the main text.

Supporting data

Age distribution in Zhejiang

According to the census data on Zhejiang [9], the age distribution on Zhejiang on the year 2020 is as follows:

304 **Distribution of family size**

305 According to the observed data, the distribution of family size is illustrated in
306 Fig. [S12](#).

307 **Age distribution by different family size**

308 According to the observed data, the age distribution on a sample of families
309 of different size is presented in Table [S2](#), in which number represents age year.

Table S1: Key parameters for the network simulation

Process	Type	Description	Value or distribution	
Social Network	Network size	The number of nodes	20,000	
	Household Connections	The average size of groups	2.94	
		Weight in household connections	Base: 3.716; Outbreak: 5.041	
	Geographical Connections	Number of geographical connections	If a node is in i th age group, the number of geographical connections of it is $2n_i$, where n_i is the average number of contacts per day of the i th age group, i.e., the sum of i th row in base contact matrix in Shanghai [4]	
		Number of geographical connections to people in each group	Multinomial distribution with the total number being $2n_i$ and the probability being the normalized i th row of base contact matrix in Shanghai.	
		Weight in geographical connections	0.5	
	Random Connections	The mean number of random connections per person	1	
		Weight in random connections	0.5	
	Transmission processes	Period	Incubation period	Log-normal(4.2, 1.9) (i.e. mean and standard deviations of the logarithms are 4.2 and 1.9 respectively) [5, 10]
			Duration on exposed state: time from being infected to being infectious	Incubation period / Log-normal(0.04, 0.59)
Pre-symptomatic infectious period			Incubation period – the duration on exposed state	
Post-symptomatic infectious period			Gamma distribution with parameter 5.2 and 8	
Removal period			Weibull distribution with mean μ_t on day t and scale $\mu_t/\Gamma(1.2)$ is assigned according to Fig. S8 (a)	
Infection rate		Infection rate per contact (β)	Peak at 5% [11] (see Table S3)	
Susceptibility		Susceptibility in each age group	See Fig. S1 [12]	
Contact number	Daily contact number to each age group	Contact matrix in each day calculated from contact matrix in Shanghai before and during the outbreak, see Fig. S3		
	The pattern of decreasing and resuming	See Fig. S3		
Imported cases	Total number of imported cases	445		
	Import day	See Fig. S8 (b)		

Table S2: Age distribution by different family size

Family size	Age distribution
2	(13, 40), (31, 32), (58, 63), (26, 49), (33, 63), (57, 61), (42, 45), (71, 74), (37, 63), (55, 72), (59, 59), (7, 36), (26, 52), (30, 35), (23, 57), (45, 47), (64, 88), (50, 53), (60, 62), (34, 35), (36, 49), (36, 40), (53, 53), (29, 58), (54, 56), (29, 51), (37, 40), (62, 71), (41, 42), (54, 55), (47, 48), (45, 69), (43, 68)
3	(32, 37, 60), (4, 10, 33), (31, 62, 85), (51, 59, 63), (7, 30, 31), (29, 37, 63), (62, 64, 66), (6, 36, 53), (0, 32, 56), (1, 34, 68), (39, 41, 43), (9, 12, 62), (36, 63, 66), (20, 44, 50), (12, 45, 45), (34, 57, 62), (51, 83, 90), (35, 56, 59), (51, 77, 79), (20, 45, 46), (38, 64, 67), (38, 40, 63), (12, 40, 43)
4	(24, 34, 41, 60), (10, 19, 41, 44), (39, 39, 66, 67), (29, 48, 51, 70), (29, 30, 31, 32), (35, 38, 67, 70), (0, 29, 51, 54), (18, 20, 42, 67), (26, 51, 80, 85), (43, 47, 70, 72), (10, 39, 39, 66), (28, 49, 51, 53), (23, 40, 49, 71)
5	(57, 58, 62, 65, 90), (11, 35, 37, 67, 69), (10, 37, 37, 38, 64), (19, 37, 44, 47, 86), (47, 48, 50, 51, 70), (31, 56, 57, 59, 85), (37, 41, 46, 47, 70), (38, 61, 64, 67, 69)
6	(13, 44, 46, 66, 74, 81), (1, 31, 32, 56, 57, 74), (22, 35, 47, 59, 60, 73)
8	(1, 22, 24, 32, 47, 56, 72, 73), (3, 6, 29, 31, 31, 32, 50, 55)
9	(21, 37, 39, 43, 43, 67, 68, 69, 72), (9, 18, 24, 37, 39, 45, 48, 67, 77)
13	(11, 27, 30, 32, 37, 56, 59, 62, 64, 64, 64, 65, 85)

Table S3: Adjusted relative risk by day from symptom onset [2] and the derived transmissibility with peak at 5%

Day ¹	Adjusted RR ²	Transmissibility	Day	Adjusted RR ²	Transmissibility
-5	0.78	0.0291	1	1.33	0.0496
-4	0.86	0.0321	2	1.27	0.0474
-3	1.02	0.0381	3	1.19	0.0444
-2	1.18	0.0440	4	1.11	0.0414
-1	1.30	0.0485	5	1.05	0.0392
0	1.34	0.0500	5	1.00	0.0373

¹ Day from symptom onset.

² RR: relative risk

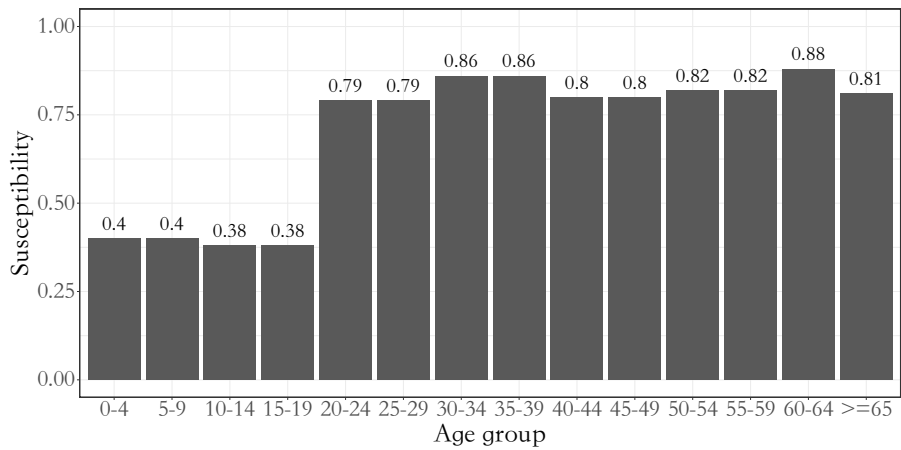


Fig. S1: Susceptibility of individuals of each age group

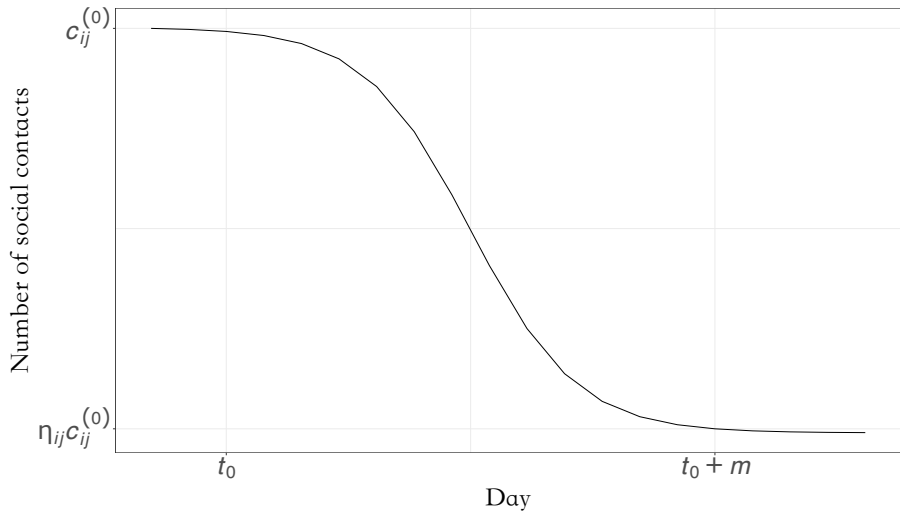


Fig. S2: Contact rates function (S1), where t_0 represents the starting time of the lock-down period, m the duration of the decreasing process, $c_{ij}^{(0)}$ the average number of social contacts between the i th and the j th age group, η_{ij} the percentage of decrease

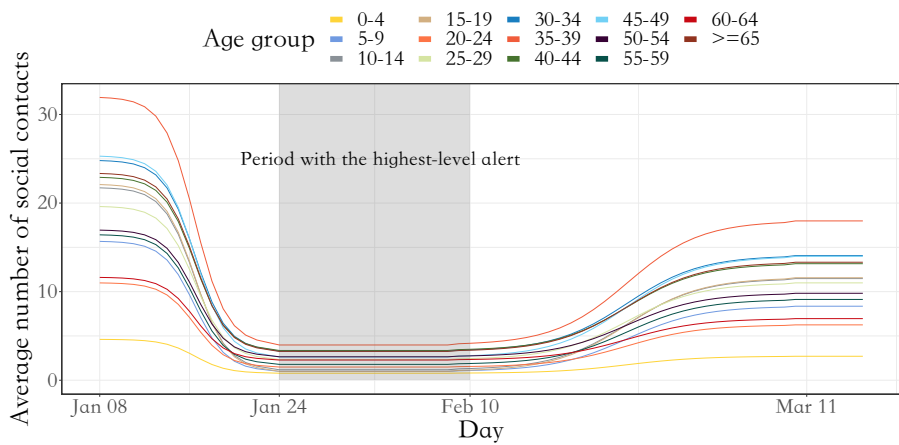


Fig. S3: Average contact number by days that is constructed based on the baseline contact matrix in Shanghai [4] and contact rates function in Fig. S2. Shaded area represents the period between January 24th and February 10th when Zhejiang was adopting highest-level response.

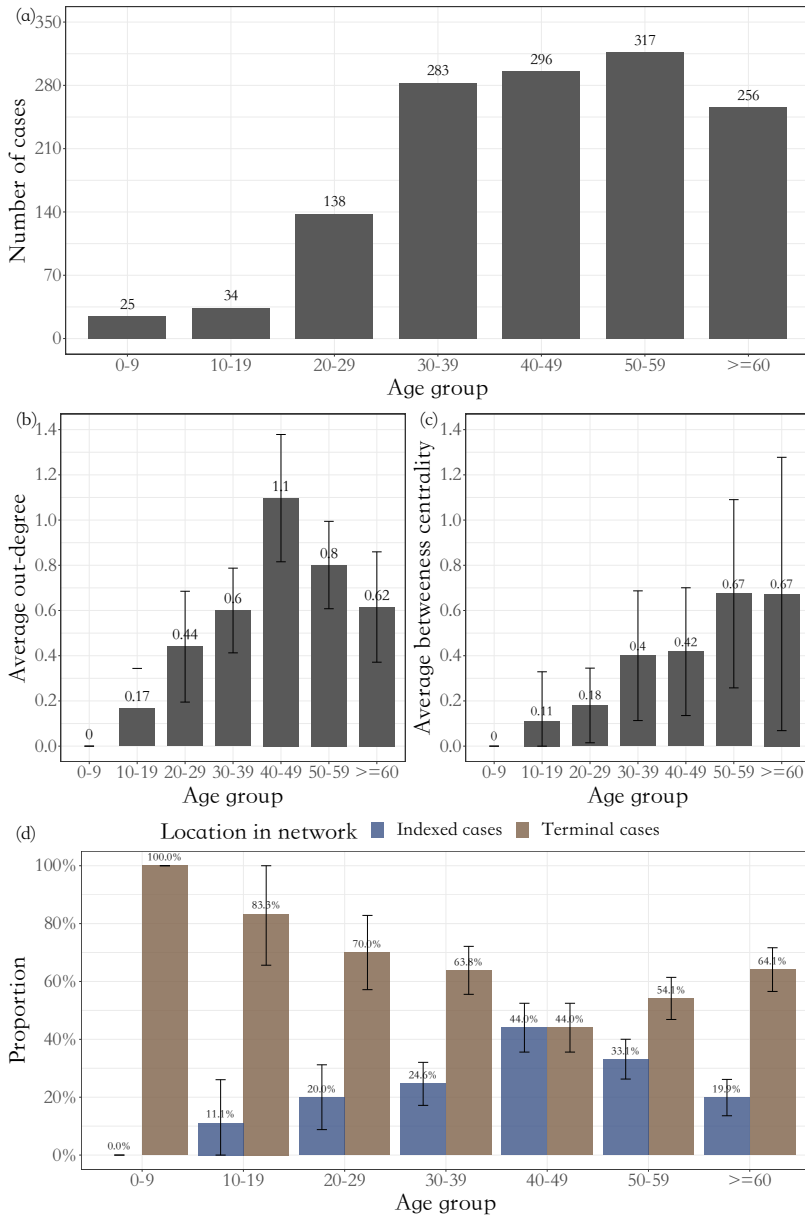


Fig. S4: (a) Number of confirmed cases in different age groups; (b) Average out-degree and 95% confidence interval of cases from each age group; (c) Average betweenness centrality and 95% confidence interval of cases from each age group; (d) Heterogeneity of cases' location in the network related to their age. If a case is the origin of a cluster, it is marked as an indexed case; if a case is positioned as the end of a cluster and thus has no further secondary infection, it is marked as a terminal case (analogous to terminal nodes in a tree).

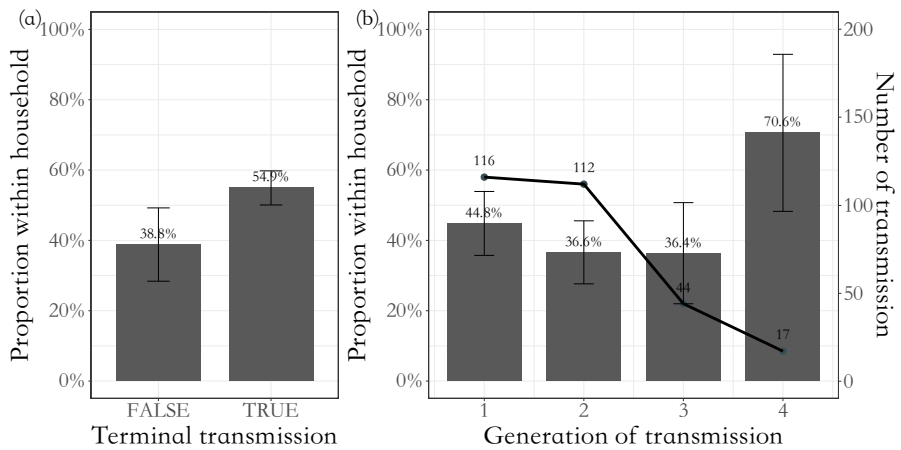


Fig. S5: (a) Proportion of household transmission with respect to whether it resulted in terminal transmission or not; (b) Proportion of household transmission with respect to the generation of transmission. If the infectee is a terminal case, the transmission pointing toward it is marked as a terminal transmission.

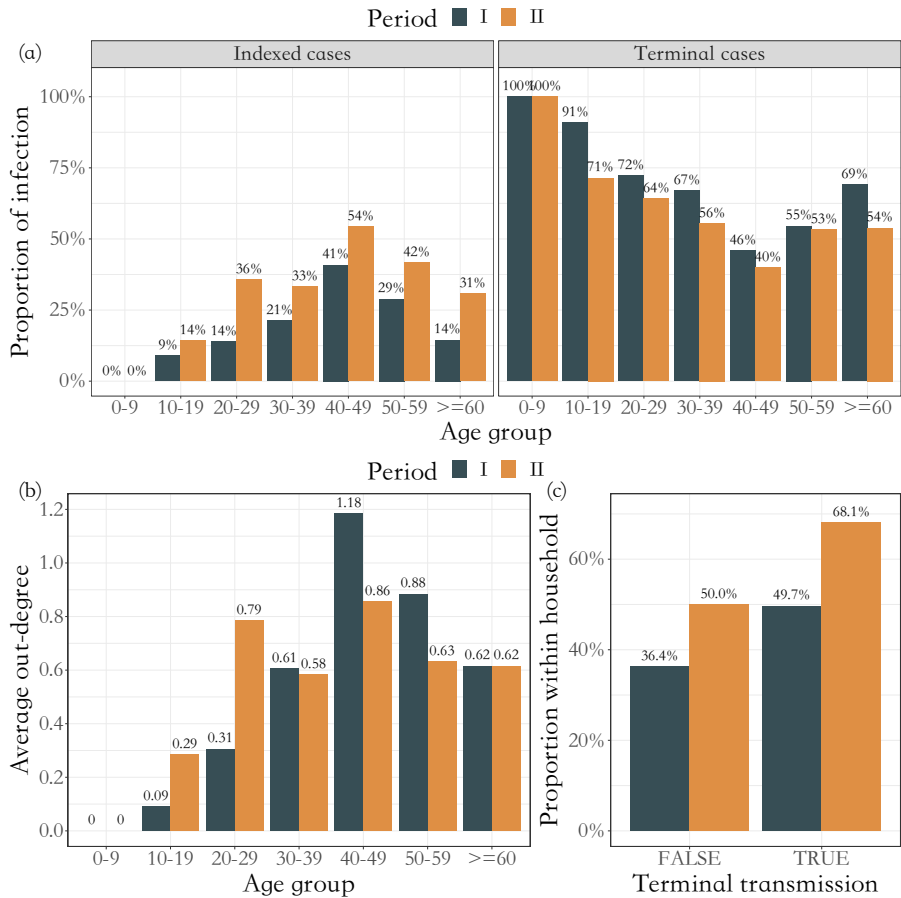


Fig. S6: (a) Heterogeneity of cases' location in the network related to their age by periods; (b) Average out-degree of cases from each age group by periods; (c) Proportion of household transmission with respect to whether terminal transmission or not by periods.

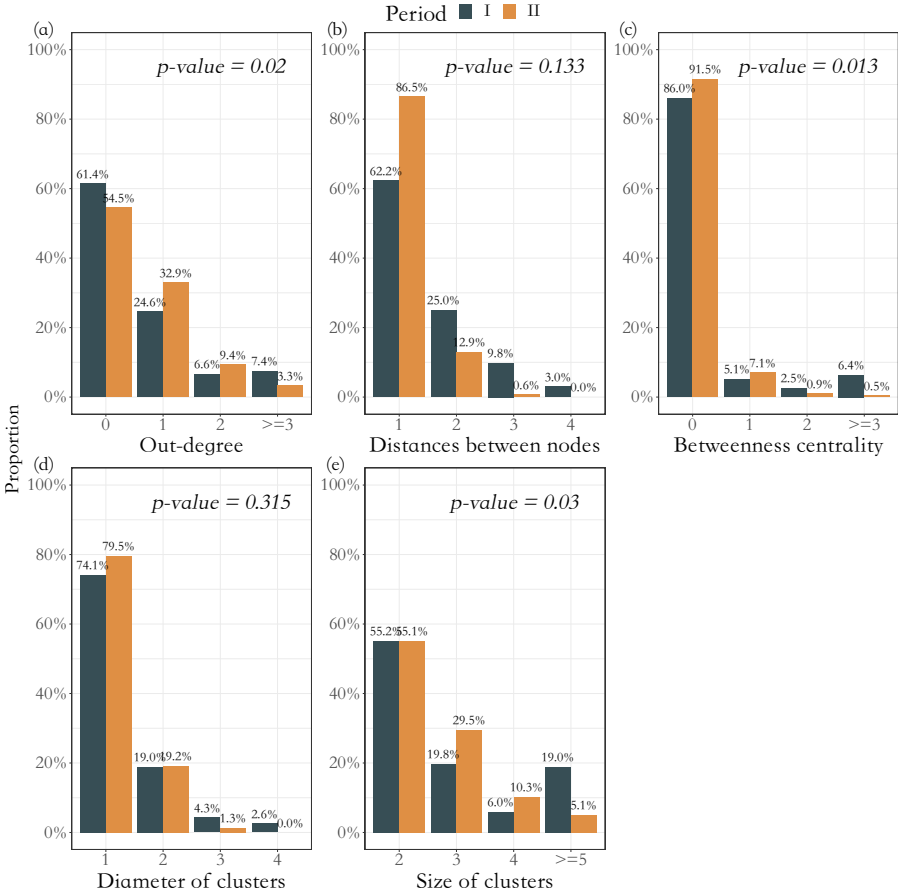


Fig. S7: Distribution of network characteristics across periods. (a) distribution of out-degree of non-singletons; (b) distribution of shortest path length; (c) distribution of betweenness centrality of non-singletons; (d) distribution of diameter of clusters; (e) distribution of size of clusters. For each network attribute, we use Pearson χ^2 test to compare the distribution across periods, and use Benjamini-Hochberg to adjust the p -values.

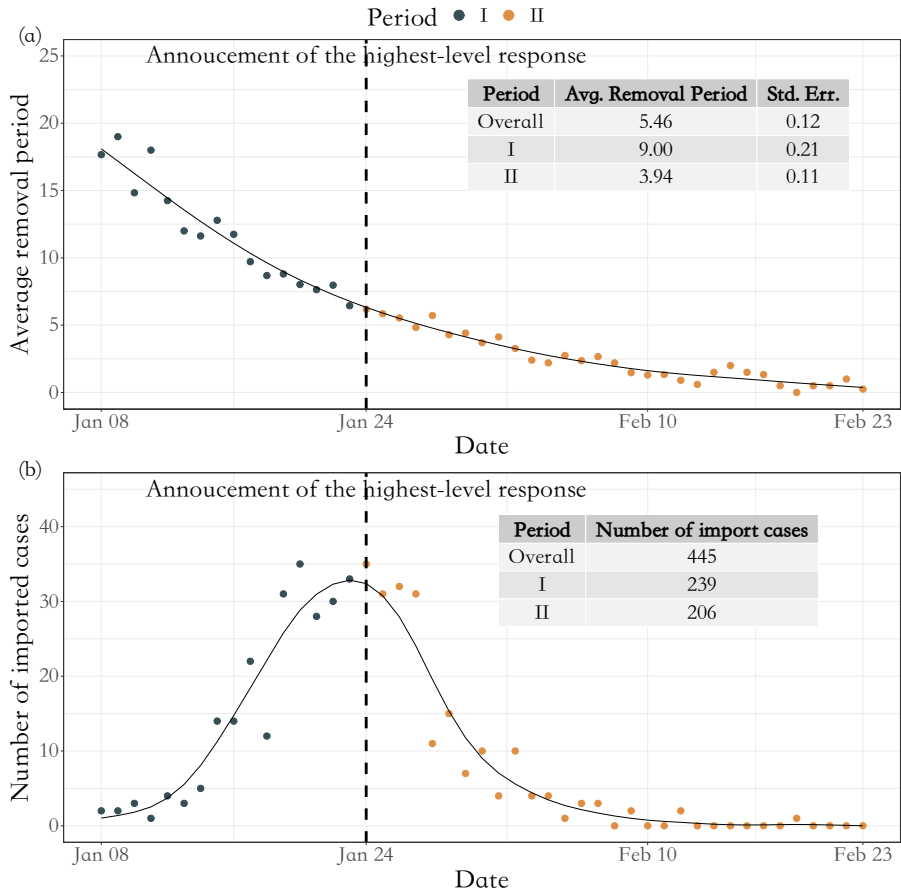


Fig. S8: (a) Average removal periods by date (b) Import cases by date

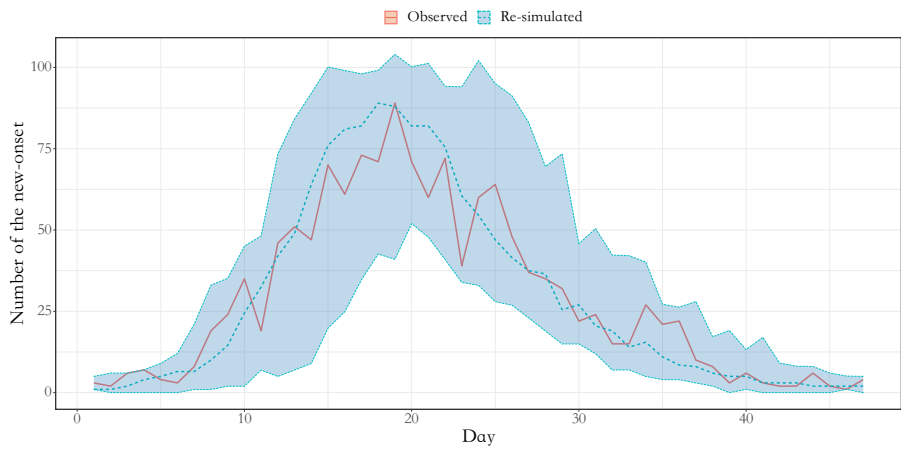


Fig. S9: Daily number of the new-onset for the observed data (line in red) and the real-data-based simulation (line in blue, the median under 200 simulations). The first day is January 8th, 2020. Blue area represents the confidence band under 200 simulations.

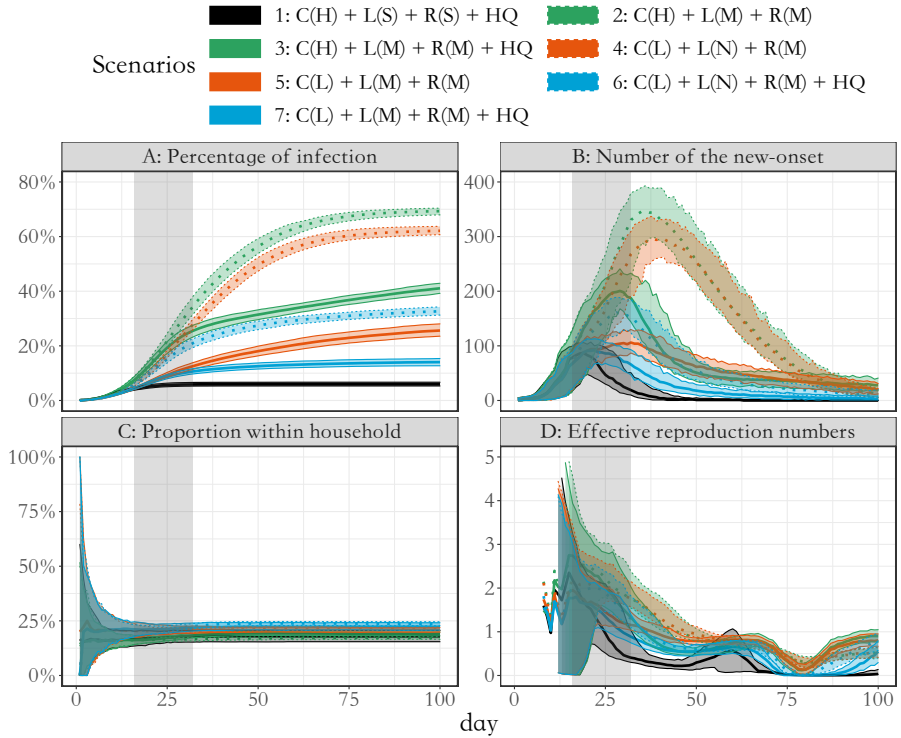


Fig. S10: Confidence band for each scenario in Fig. 7, obtained from 200 simulations.

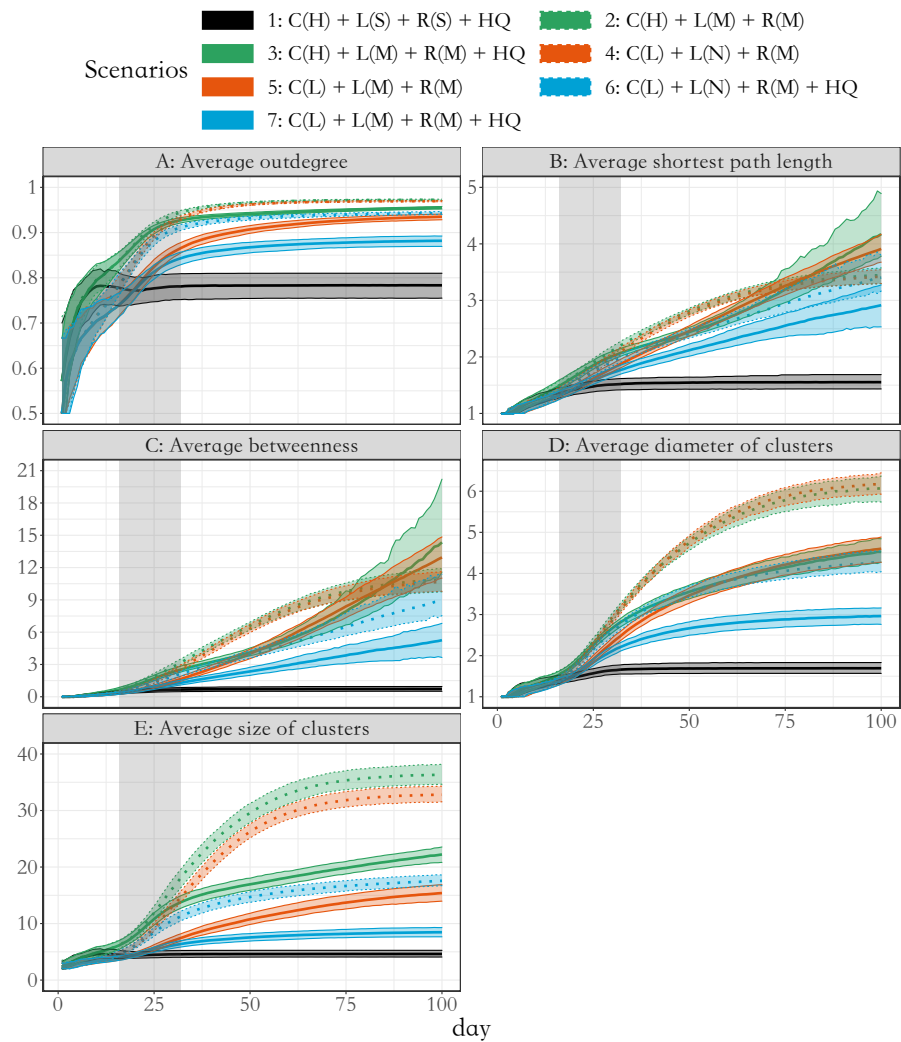


Fig. S11: Confidence band for each scenario in Fig. 8, obtained from 200 simulations.

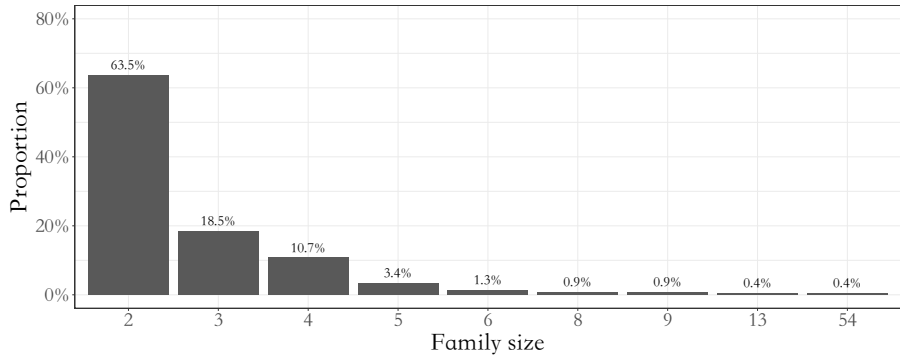


Fig. S12: The distribution of family size. The average family size is 2.94 (SE: 0.24)

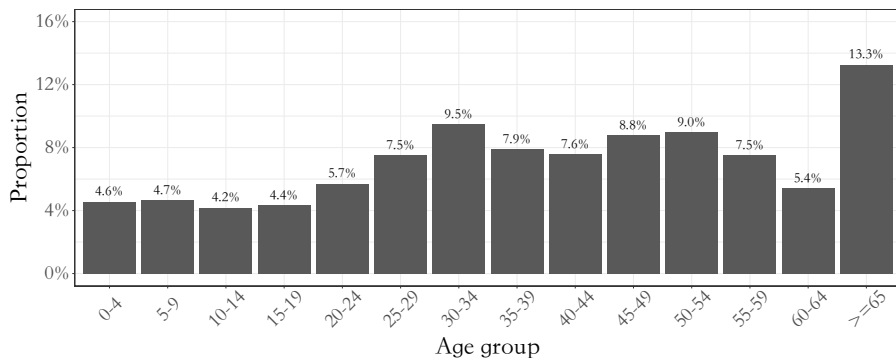


Fig. S13: Age distribution on Zhejiang on the year 2020

References

- 310
- 311 [1] Shen, Y. *et al.* Community outbreak investigation of sars-cov-2 trans-
 312 mission among bus riders in eastern china. *JAMA Internal Medicine*
 313 **180** (12), 1665–1671 (2020) .
- 314 [2] Ge, Y. *et al.* Covid-19 transmission dynamics among close contacts of
 315 index patients with covid-19: A population-based cohort study in zhejiang
 316 province, china. *JAMA Internal Medicine* (2021) .
- 317 [3] Mao, G. & Zhang, N. Analysis of average shortest-path length of scale-free
 318 network. *Journal of Applied Mathematics* **2013** (2013) .
- 319 [4] Zhang, J. *et al.* Changes in contact patterns shape the dynamics of the
 320 covid-19 outbreak in china. *Science* **368** (6498), 1481–1486 (2020) .
- 321 [5] He, X. *et al.* Temporal dynamics in viral shedding and transmissibility of
 322 covid-19. *Nature Medicine* **26** (5), 672–675 (2020) .
- 323 [6] Seah, I. Y. J. *et al.* Assessing viral shedding and infectivity of tears in
 324 coronavirus disease 2019 (covid-19) patients. *Ophthalmology* **127** (7), 977
 325 (2020) .
- 326 [7] Nande, A., Adlam, B., Sheen, J., Levy, M. Z. & Hill, A. L. Dynamics
 327 of covid-19 under social distancing measures are driven by transmission
 328 network structure. *PLoS Computational Biology* **17** (2), e1008684 (2021) .
- 329 [8] Tan, J. *et al.* Transmission roles of symptomatic and asymptomatic covid-
 330 19 cases: a modeling study. *medRxiv* 2021.05.11.21257060 (2021) .
- 331 [9] Tongjiju, Z. & DiaochaZongdui, G. T. *Zhejiang tongji nianjian-2021*
 332 [*Statistical yearbook of Zhejiang-2021*] (China Statistic Publishing House,

- 333 Zhejiang, China, 2021).
- 334 [10] Li, Q. *et al.* Early transmission dynamics in wuhan, china, of novel coron-
335 avirus-infected pneumonia. *New England Journal of Medicine* **382** (13),
336 1199–1207 (2020) .
- 337 [11] Nishi, A. *et al.* Network interventions for managing the covid-19 pandemic
338 and sustaining economy. *Proceedings of the National Academy of Sciences*
339 **117** (48), 30285–30294 (2020) .
- 340 [12] Davies, N. G. *et al.* Age-dependent effects in the transmission and control
341 of covid-19 epidemics. *Nature Medicine* **26** (8), 1205–1211 (2020) .